Attenuation of the Dynamic Yield Point of Shocked Aluminum Using Elastodynamic Simulations of Dislocation Dynamics

Beñat Gurrutxaga-Lerma, Daniel S. Balint, and Daniele Dini

Department of Mechanical Engineering Imperial College London, London SW7 2AZ, United Kingdom

Daniel E. Eakins and Adrian P. Sutton

Department of Physics Imperial College London, London SW7 2AZ, United Kingdom

When a metal is subjected to extremely rapid compression, a shock wave is launched that generates dislocations as it propagates. The shock wave evolves into a characteristic two-wave structure, with an elastic wave preceding a plastic front. It has been known for more than six decades that the amplitude of the elastic wave decays the farther it travels into the metal: this is known as "the decay of the elastic precursor." The amplitude of the elastic precursor is a dynamic yield point because it marks the transition from elastic to plastic behavior. In this Letter we provide a full explanation of this attenuation using the first method of dislocation dynamics to treat the time dependence of the elastic fields of dislocations explicitly. We show that the decay of the elastic precursor is a result of the interference of the elastic shock wave with elastic waves emanating from dislocations nucleated in the shock front. Our simulations reproduce quantitatively recent experiments on the decay of the elastic precursor in aluminum and its dependence on strain rate.

The dynamic behavior of crystalline solids subjected to shock compression plays a central role in diverse applications, including bird strikes in aerospace [1], crashworthiness in the automobile industry [2], and manufacturing processes such as laser shock peening [3], among many others. Upon being shocked within a range of strain rates and pressures of typically 10^6–10^{10} s^{-1} and 5–50 GPa [1], the shock front in crystalline materials often displays a characteristic two-wave structure near the loading surface: the plastic wave front leading to the Hugoniot shocked state is preceded by an elastic precursor wave [1]. The amplitude of the elastic precursor wave decays as the wave front advances [1,4]—a phenomenon known as the "decay of the elastic precursor." The amplitude of the elastic wave marks the onset of plasticity; i.e., it is the dynamic yield point. The subsequent plastic wave is commonly ascribed to the generation and motion of dislocations, the agents of plasticity in crystalline solids [5].

The cause of its attenuation remains unclear after six decades [4,6–9]. Clifton and Markenscoff [4] calculated analytically the amplitude attenuation of a planar elastic shock wave caused by the destructive interference of elastic wavelets emanating from preexisting dislocations set into motion by the passage of a shock wave of infinite strain rate; dislocation generation by the shock was neglected. Consequently, the elastic precursor decay was attributed to the density and initial velocity of preexisting dislocations. Armstrong *et al.* [10] studied the dislocation relaxation mechanisms during high strain rate shock loading, concluding that dislocation generation dominates plastic relaxation under shock loading.

In this Letter we show that we can account for the experimentally observed residual dislocation densities created by shock loading by assuming no preexisting dislocations and that dislocations are generated within and behind the shock front. The material is assumed to be initially dislocation free because the number of preexisting dislocations is about 2–3 orders of magnitude less than that generated during the shock [1,4,8]. We go on to offer a complete explanation of the attenuation of the dynamic yield point, employing our recently developed method of dynamic discrete dislocation plasticity (D3P) [11]. Modern computing resources enable the simulation of crystalline metals subjected to shock loading using molecular dynamics (MD) simulations [12–14], but these are unable to discriminate between the effects of dislocations and other mechanisms in plastic relaxation processes. In contrast to MD, discrete dislocation dynamics methods [15–18] enable the simulation of much larger systems over longer time scales. However, conventional discrete dislocation dynamics methods are inappropriate for the study of high strain rate shock compression, because they neglect the time dependence of the fields of moving dislocations. We showed in Ref. [11] that at high strain rates this leads to violation of causality because dislocation sources may be activated ahead of the shock.

We compare our simulations with a series of shock compression experiments performed at room temperature on an equivalent length and time scale. In these experiments, a range of μm-scale polycrystalline aluminum films were subjected to shock loading using a spectrally shaped laser pulse (Fig. 1). The development of the two-wave
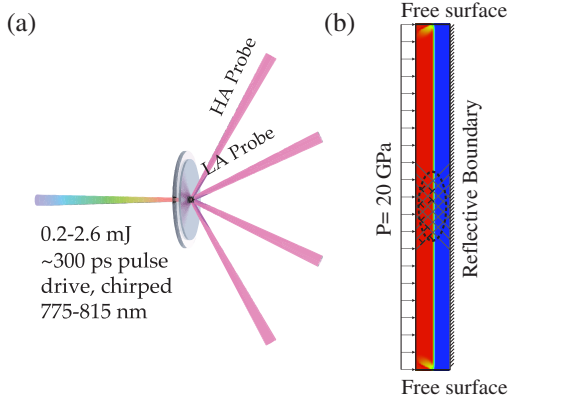
FIG. 1 (color online). (a) Experimental setup and (b) D3P simulation. HA stands for high angle probe, LA for low angle probe.
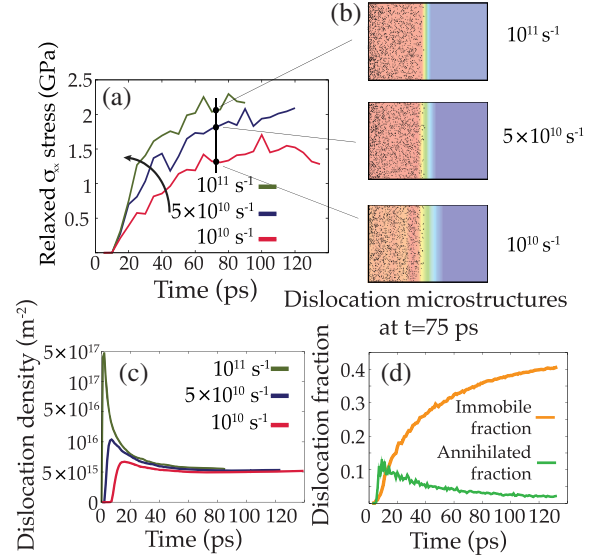

FIG. 2 (color online). (a) Accumulated relaxation effect of the dislocation fields at the shock front, for different strain rates. (b) Dislocation microstructures for different strain rates at $t = 75$ ps. (c) Increase in ρ_{dis} with the strain rate. (d) Immobile and annihilated fractions of dislocations for 10^{10} s^{-1}.

structure was probed using a pair of off-axis displacement interferometers, with time resolution approaching several picoseconds. By maintaining a constant drive energy and varying the film thickness, the yield point was observed to decay from 12 GPa for 2 μm to 4.3 GPa after 8 μm [19].

Our D3P model simulates a single crystal sample of fcc aluminum at room temperature depicted in Fig. 1, with Young's modulus $E = 63.2$ GPa, shear modulus $\mu = 28.3$ GPa, density $\rho = 2700$ kg/m^3, and Burgers vector $b = (a\sqrt{2}/2) = 2.85$ Å. The sample is 10 μm wide and 1 μm thick. Following Ref. [20], we assume 3 slip planes at $\pm 54.7°, 0°$ to the shock front's normal. The sample is initially dislocation free, and loaded with an instantaneous 20 GPa pressure on its left side. A reflective boundary condition is applied on the right side, whereas the top and bottom sides are left traction free. Because of the loading, a shock front is generated and propagates through the material, triggering dislocation activity. The simulation finishes when the front reaches the reflective surface. The strain rate is enforced numerically (see Supplemental Material [21]).

D3P tracks the time-dependent fields of injected and nonuniformly moving straight edge dislocations by solving the Navier-Lamé equation under plane strain conditions. Elastic nonlinearities and core effects are not considered. Plane strain is a reasonable approximation here since a strongly uniaxial compressive shock load is applied over a relatively large area, orders of magnitude thinner in the direction of propagation. In D3P, the resulting elastic fields propagate at the two speeds of sound [11], which ensures that causality is satisfied.

We assume the generation and motion of dislocations follows the constitutive rules of D3P [11]. The mobility law of dislocations is adjusted to account for the likely presence of high-speed dislocations [1,18,30–36]; data about the mobility of dislocations are extracted from MD simulations of aluminum [37] (see Supplemental Material [21]).

Two generation mechanisms are allowed: homogeneous nucleation and Frank-Read sources. At high strain rates Frank-Read sources are too slow with respect to the shock front's rise time to play a significant role in generating dislocations (see Supplemental Material [21]). Thus, faster dislocation generation mechanisms must be considered. Smith [38], Hornbogen [39], Meyers and co-workers [40,41], Shehadeh et al. [42] (using elastostatics) and Armstrong et al. [30] have all proposed dislocation generation processes involving homogeneous nucleation. Recent simulations show that the stress levels required to nucleate dislocations homogeneously are about the ideal shear lattice resistance $[\mu/18 - \mu/(4\pi)]$, easily achievable in shock loading (see Refs. [43–45]). Recent MD simulations [14,46] also suggest that homogeneous nucleation is a primary source of dislocation loops, particularly for strain rates larger than 10^8–10^9 s^{-1} [46]. Here, homogeneous nucleation sources are assumed to operate instantaneously with activation stresses much higher that those for Frank-Read sources (see Supplemental Material [21]).

We report a series of simulations in which the initial shock's amplitude was constant at 20 GPa. These simulations concern the study of the elastic precursor and the early onset of the plastic wave. By varying the shock's width, three strain rates were imposed: 10^{10}, 5×10^{10}, and 10^{11} s^{-1}. These strain rates are close to those found by Crowhurst et al. [47] to lead to overdriven shocks, but still under the weak shock regime. Figure 2 shows the σ_{xx} fields of dislocations, measured by averaging their elastodynamic stresses along a line parallel to the front and immediately behind it; its positive (tensile) magnitude interferes with the

front's negative (compressive) amplitude. The elastic precursor decay is obtained by subtracting the corresponding curve shown in Fig. 2 from a reference hyperelastic state. Figure 2 is consistent with experimental observation that the rate of decay increases with the strain rate [48]. Here the strain rate's effect is not entirely comparable to experiment, as in the latter the magnitude of the shock itself would vary, too [49]. Nevertheless, Fig. 2 shows that an increase in the strain rate invariably leads to a higher relaxation of the shock; for the same time interval, a higher strain rate signifies that a larger area is subjected to higher stresses, resulting in a higher number of dislocations being generated within the front. As discussed below, there is a further significant contribution to the relaxation from the velocity dependence of the dislocations' elastic fields.

Figure 2 also shows the evolution of the dislocation density (ρ_{dis}) for the three strain rates, calculated as the number of dislocations in the system at time t divided by the area swept by the front up to t. In Fig. 2 ρ_{dis} tends to saturate after an initial burst. The decay from this initial burst is a geometric effect: the number of dislocations tends to increase in proportion to the height of the sample, but the area behind the front increases in proportion to both the sample height and $c_l t$. Following this burst, dislocation dipoles are generated at a reduced steady rate, which leads to the saturated ρ_{dis} seen in Fig. 2.

The computed $\rho_{\mathrm{dis}} \approx 6 \times 10^{15}$ m^{-2} is of the same order of magnitude as that measured experimentally [1], and comparable to that predicted by analytical models such as that by Meyers *et al.* [41], which predicts a $\rho_{\mathrm{dis}} = 2.5 \times 10^{15}$ m^{-2} for aluminum shocked at 20 GPa. The dislocation structures at the front (see Fig. 4) resemble those expected from the classical Smith-Hornbogen interface [30,38,39], with positive "shielding" dislocations trailing just behind the front and negative "antishielding" dislocations moving rapidly away from it. However, the nucleation process here is much more gradual, as it accounts for the strain rate of the shock front, and takes place not only at the front but behind it.

At these strain rates, Frank-Read sources have no effect on the elastic precursor decay. With ≈ 40 ps activation times, they can generate only two or three dipoles throughout the simulation, and they are activated long after the front has passed; thus, the elastic fields of the newly generated dislocations cannot influence the front. We find the number of dislocations nucleated homogeneously is 2 orders of magnitude larger than those generated by Frank-Read sources. These results indicate that the relative contribution of each of these mechanisms of dislocation generation depends on the strain rate.

Figure 2 shows the evolution of the immobile fraction of dislocations, defined as those that move at speeds less than 100 m/s. After 120 ps this fraction increases to 40%–45%. Thus, a significant fraction of the dislocations are effectively halted due to the sudden increase in ρ_{dis} in the wake of the front. Figure 2 also shows the number of annihilated

dislocations. Most annihilations correspond to dipoles that are nucleated homogeneously with separations between the dislocations too small to overcome their mutual attraction. As the front proceeds, it is seen that an increasing fraction of dislocations survives.

Figure 3 shows a comparison of the experimental data for aluminum at 10^{10} s^{-1} and our simulated results up to 350 ps at the same strain rate. To simulate the longer times, the longitudinal sample size had to be increased from 1 to 3.5 μm while keeping the lateral dimension 10 μm; the aspect ratio is enough to ensure that release waves do not reach the midsections. The simulations were not extended further owing to computational limitations associated with longer time scales. The decay with time of the elastic precursor can be fitted to $f(t) = A e^{-mt}$. The logarithmic decay rate is defined as $m = -[(1/f)(df/dt)]$. With a strain rate of 10^{10} s^{-1}, we obtain in our simulations $m = 0.0012 \pm 0.0002$. The experimental data for aluminum obtained by Whitley *et al.* [19] for a strain rate of 10^{10} s^{-1} yield a logarithmic decay rate of $m = 0.001259$.

When a dipole is generated within the shock front, one dislocation of each dipole has a velocity component antiparallel to the shock front's velocity, and its stress wave is antishielding [50] because it constructively interferes with the shock front's compressive amplitude. The other dislocation, with a velocity component parallel to the front's velocity, is a shielding dislocation, as it destructively interferes with (decreases) the front's compressive amplitude. The cumulative effect of the shielding dislocations is greater than the effect of the antishielding dislocations, because the former are within the front for much longer. Thus, as first suggested by Clifton and Markenscoff [4], the cause of the elastic precursor decay is the cumulative and destructive interference of elastic waves emanating from shielding dislocations at the shock front. In this work, dislocations are nucleated within the front, while in Ref. [4] they were preexisting.
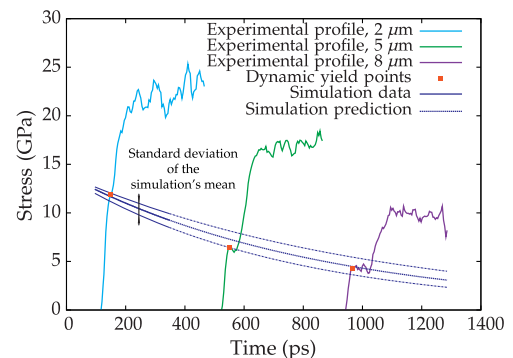

FIG. 3 (color online).   Experimental versus simulated decay rate. The solid blue line is an exponential fit to our simulations; its extrapolation beyond 350 ps is shown as a broken line. The broken lines on either side of this fit represent the standard deviation of the simulation's mean from the fit.
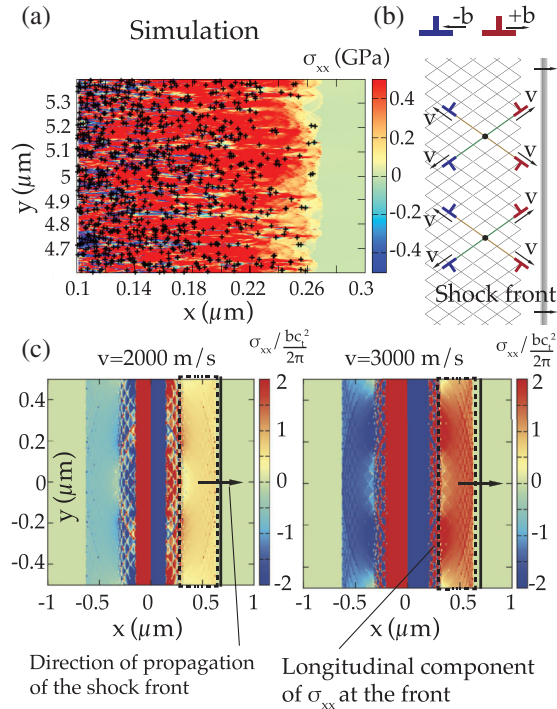
FIG. 4 (color online). (a) Dislocation structure and its associated σ_{xx} field. (b) Dislocation structure is idealized by the Smith-Hornbogen interface. Red dislocations are shielding, blue are antishielding. (c) σ_{xx} fields of the idealized dislocation configuration seen in (b).

The destructive interference is greater at larger strain rates. Figure 4(a) shows a snapshot of the dislocation structure at the front at $t = 60$ ps, together with their σ_{xx} fields, with $\dot{\epsilon} = 10^{10}$ s^{-1}. The dislocations in Fig. 4(a) are seen to organize themselves in structures reminiscent of a Smith-Hornbogen interface [30,38,39]; this results in a net plastic relaxation of the compressive elastic shock front. Figure 4(b), idealizes the dislocation structure to a Smith-Hornbogen interface, with shielding dislocations moving frontwards and antishielding dislocations moving away from the front [shown, respectively, in red and blue in Fig. 4(b)]. Figure 4(c) shows the σ_{xx} fields of a single Smith-Hornbogen interface for two different dislocation speeds, 2000 and 3000 m/s, assuming all dislocations move with the same speed. Because the shock front propagates with c_l, only the longitudinal wave component of each dislocation's field can keep up with the front and contribute to the plastic relaxation of the shock wave.

An analysis of the longitudinal component of the σ_{xx} field in Fig. 4(c) shows that its magnitude almost doubles when the dislocations' speed increases from $v_{dis} = 2000$ m/s to $v_{dis} = 3000$ m/s. This arises from the contraction of the dislocation fields in the direction of motion as v_{dis} increases. The contraction exists only ahead of the dislocation, in the direction of motion; behind the dislocation the magnitude of its fields tends to decrease. Consider the shielding dislocations: with increasing speed, the magnitude of the

longitudinal component of σ_{xx} increases ahead of the dislocations, contributing to a greater relaxation of the shock front; this effect persists longer because the dislocations are moving faster towards the shock front. For antishielding dislocations, since they move away from the front, increasing their speed results in a relative decrease in the magnitude of the longitudinal component of σ_{xx} influencing the front. Because they move faster away from the front, they influence the shock front for less time. As a result, the amplitude of the shock wave is reduced much more by the shielding dislocations than it is increased by the antishielding dislocations, and this effect is magnified by increasing the strain rate.

We conclude that the dynamic yield stress is determined by an interference phenomenon between the elastic precursor wave and the elastic waves of shielding dislocations generated at the front. The increasing attenuation of the dynamic yield point with increasing strain rate (see Fig. 2) is a direct result of the elastodynamic fields of moving dislocations. This insight has been achieved by simulating the elastodynamic fields of dislocations nucleated and propagating as a result of the shock, a unique feature of D3P. Using D3P we have also explained the increasing attenuation of the dynamic yield stress with increasing strain rate within the shock.

Our results highlight the importance of dislocation generation mechanisms in relaxation processes at very high strain rates. Although at the strain rates probed here Frank-Read sources are generally too slow to be activated before the front is relaxed by homogeneously nucleated dislocations, it seems possible they may be involved in relaxation at much lower strain rates via the same mechanism.

[1] M. Meyers, *Dynamic Behavior of Materials* (John Wiley, New York, 1994).
[2] S. Hiermaier, *Structures under Crash and Impact* (Springer, New York, 2007).
[3] C. Montross, T. Wei, L. Ye, G. Clark, and Y.-W. Mai, International Journal of Fatigue **24**, 1021 (2002).
[4] R. Clifton and X. Markenscoff, J. Mech. Phys. Solids **29**, 227 (1981).
[5] J. Hirth and J. Lothe, *Theory of Dislocations*, 2nd ed. (Krieger, Melbourne, Florida, 1991).
[6] J. Campbell, Acta Metall. **1**, 706 (1953).
[7] J. Taylor, J. Appl. Phys. **36**, 3146 (1965).
[8] Y. Partom, J. Appl. Phys. **59**, 2716 (1986).
[9] B. J. Demaske, V. V. Zhakhovsky, N. A. Inogamov, and I. I. Oleynik, Phys. Rev. B **87**, 054109 (2013).
[10] R. Armstrong, W. Arnold, and F. Zerilli, J. Appl. Phys. **105**, 023511 (2009).
[11] B. Gurrutxaga-Lerma, D. Balint, D. Dini, D. Eakins, and A. Sutton, Proc. R. Soc. A **469**, 20130141 (2013).

[12] V. Bulatov, F. Abraham, L. Kubin, B. Devincre, and S. Yip, Nature (London) **391**, 669 (1998).

[13] E. Bringa, A. Caro, Y. Wang, M. Victoria, J. McNaney, B. Remington, R. Smith, B. Torralva, and H. Van Swygenhoven, Science **309**, 1838 (2005).

[14] E. Bringa, K. Rosolankova, R. Rudd, B. Remington, J. Wark, M. Duchaineau, D. Kalantar, J. Hawreliak, and J. Belak, Nat. Mater. **5**, 805 (2006).

[15] E. Van der Giessen and A. Needleman, Model. Simul. Mater. Sci. Eng. **3**, 689 (1995).

[16] L. Kubin and G. Canova, Scr. Metall. **27**, 957 (1992).

[17] V. Bulatov and W. Cai, *Computer Simulations of Dislocation* (Oxford University Press, Oxford, England, 2006).

[18] M. Shehadeh, H. Zbib, and T. Diaz de la Rubia, Int. J. Plast. **21**, 2369 (2005).

[19] V. Whitley, S. McGrane, D. Eakins, C. Bolme, D. Moore, and J. Bingert, J. Appl. Phys. **109**, 013505 (2011).

[20] J. Rice, Mech. Mater. **6**, 317 (1987).

[21] See Supplemental Material at http://link.aps.org/supplemental/10.1103/PhysRevLett.114.174301, which includes Refs. [22–29], for a detailed description and justification of the methodological assumptions the simulations are based on.

[22] V. Lubarda, J. Blume, and A. Needleman, Acta Metall. Mater. **41**, 625 (1993).

[23] O. Zienkiewicz, *The Finite Element Method: Its Basis and Fundamentals*, 6th ed. (Butterworth-Heinemann, Washington, DC, 2005).

[24] T. Mura, *Micromechics of Defects in Solids*, 1st ed. (Martinus Nijhoff, The Hague, 1982).

[25] A. Benzerga, Y. Bréchet, A. Needleman, and E. Van der Giessen, Model. Simul. Mater. Sci. Eng. **12**, 159 (2004).

[26] A. Benzerga, Int. J. Plast. **24**, 1128 (2008).

[27] S. Shishvan and E. Van der Giessen, J. Mech. Phys. Solids **58**, 678 (2010).

[28] X. Markenscoff, J. Elast. **10**, 193 (1980).

[29] C. Teodosiu, *Elastic Models of Crystal Defects* (Springer-Verlag, London, 1982).

[30] R. Armstrong, W. Arnold, and F. Zerilli, Metall. Mater. Trans. A **38**, 2605 (2007).

[31] J. Hirth, H. Zbib, and J. Lothe, Model. Simul. Mater. Sci. Eng. **6**, 165 (1998).

[32] L. Pillon, C. Denoual, and Y. P. Pellegrini, Phys. Rev. B **76**, 224105 (2007).

[33] Y. P. Pellegrini, Phys. Rev. B **90**, 054120 (2014).

[34] R. J. Beltz, T. L. Davis, and K. Malén, Phys. Status Solidi B **26**, 621 (1968).

[35] P. Gillis and J. Kratochvil, Philos. Mag. **21**, 425 (1970).

[36] H. Zbib and T. Diaz de la Rubia, Int. J. Plast. **18**, 1133 (2002).

[37] D. Olmsted, L. Hector, W. Curtin, and R. Clifton, Model. Simul. Mater. Sci. Eng. **13**, 371 (2005).

[38] C. Smith, Trans. Metall. Soc. AIME **212**, 574 (1958).

[39] E. Hornbogen, Acta Metall. **10**, 978 (1962).

[40] M. Meyers, Scr. Metall. **12**, 21 (1978).

[41] M. Meyers, F. Gregori, B. Kad, M. Schneider, D. Kalantar, B. Remington, G. Ravichandran, T. Boehly, and J. Wark, Acta Mater. **51**, 1211 (2003).

[42] M. A. Shehadeh, E. M. Bringa, H. M. Zbib, J. M. McNaney, and B. A. Remington, Appl. Phys. Lett. **89**, 171918 (2006).

[43] M. Tschopp and D. McDowell, J. Mech. Phys. Solids **56**, 1806 (2008).

[44] M. Y. Gutkin and I. A. Ovid'ko, Acta Mater. **56**, 1642 (2008).

[45] S. Aubry, K. Kang, S. Ryu, and W. Cai, Scr. Mater. **64**, 1043 (2011).

[46] B. L. Holian and P. S. Lomdahl, Science **280**, 2085 (1998).

[47] J. C. Crowhurst, M. R. Armstrong, K. B. Knight, J. M. Zaug, and E. M. Behymer, Phys. Rev. Lett. **107**, 144302 (2011).

[48] R. Rohde, Acta Metall. **17**, 353 (1969).

[49] D. Grady, J. Appl. Phys. **107**, 013506 (2010).

[50] R. Thomson, *Physics of Fracture* (Academic Press, London, 1986), pp. 1–129.

[51] J. Gilman, *Micromechanics of Flow in Solids* (McGraw-Hill, New York, 1969).